Proceedings of the 49th International School and Conference on the Physics of Semiconductors "Jaszowiec 2021"

Voltage- and Frequency-Dependent Electrical Characteristics and Interface State Density of Ni/ZnO Schottky Diodes

S.M. Faraz[a,*], Z. Tajwar[a], Q. ul Wahab[b], A. Ulyashin[c] and R. Yakimova[b]

[a] *Department of Electronic Engineering, NED University of Engineering and Technology, University Road, 75270, Karachi, Pakistan*
[b] *Department of Physics, Chemistry and Biology, Linköping University, 58183 Linköping, Sweden*
[c] *SINTEF Industry Forskingsveien 1, 0314 Oslo, Norway*

Doi: 10.12693/APhysPolA.141.99 *e-mail: smuniza@neduet.edu.pk

Frequency and voltage dependent electrical characteristics are reported for Ni/ZnO Schottky diodes. Schottky diodes are realized from nano-structured ZnO thin films grown by DC magnetron sputtering. Electrical characterizations are performed by current–voltage (I–V), capacitance–voltage (C–V) and conductance–voltage (G/ω–V) measurements. The diode parameters are extracted, such as barrier height (ϕ_B), ideality factor (n) and carrier concentration (N_D). The diodes exhibited a non-linear rectifying behaviour with a barrier height of 0.68 eV and an ideality factor greater than unity. Charge transport mechanism and possible reasons responsible for non-idealities are investigated. The density of interface states (N_{SS}) below the conduction band are extracted from the measured values of I–V and C–V as a function of $E_C - E_{SS}$. From $E_C - 0.51$ to $E_C - 0.64$ eV below the conduction band edge, the interface state density N_{SS} is found to be in the range 1.74×10^{12}–1.87×10^{11} eV^{-1} cm^{-2}. The interface states density obtained from capacitance–frequency (C–f) characteristics varied from 0.53×10^{12}–0.12×10^{12} eV^{-1} cm^{-2} from $E_C - 0.82$ eV to $E_C - 0.89$ eV below the conduction band. A complete description of current transport and interface properties is important for the realization of good quality Schottky diodes and for the design and implementation of high performance electronic circuits and systems.

topics: ZnO Schottky diode, Interface states, DC magnetron sputtering

1. Introduction

Zinc Oxide (ZnO) is a group II–VI metal oxide semiconductor with a direct and wide bandgap (3.37 eV) and large exciton binding energy (60 meV). It is a biosecure and cost effective semiconductor with good thermal and chemical stability. Moreover, it has a rich family of nanostructures which can be grown easily on a variety of substrates using numerous synthesis and deposition techniques such as sol–gel, hydrothermal, spray pyrolysis, thermal evaporation, pulsed laser deposition, chemical vapour deposition, RF and DC Magnetron sputtering [1–5]. Because of its high conductivity and good transparency, ZnO is considered as a promising material for electronic and photonic devices like UV detectors, sensors, MEMs, LEDs, solar cells, heterojunctions and Schottky diodes [6–12].

Schottky diodes are the basis of a wide range of electronic applications in rectifiers, switches, mixers and power electronics. ZnO Schottky contacts can be realized of metal with high work functions such as platinum (Pt), palladium (Pd), nickel (Ni), gold (Au), silver (Ag) and copper (Cu) etc. Yadav et al. [13] and Ahmed et al. [14] achieved a rectification from three to five orders of magnitude from Pd/ZnO Schottky contacts fabricated by the sol–gel technique. Similarly, Au/ZnO Schottky contacts with excellent rectifying characteristics are reported by Aydoğan et al. [15] and Shokri et al. [16], for potential applications as electrodes for thermoelectric devices, gas sensors and dye-sensitized solar cells. In the same way, Singh et al. [17] compared the performance of Pd and Au Schottky contacts on ZnO deposited by RF magnetron sputtering, where the Pd/ZnO Schottky diodes outperformed the Au/ZnO diodes by ideality factor and barrier height. A superior photoconductivity and improved electrical behaviour of Pd/ZnO and Ag/ZnO Schottky diodes is reported in several studies [18–20]. The Schottky diode of ZnO with Pt are also found to exhibit a linear response with a variation in hydrogen concentration, which indicates a potential for applications in hydrogen gas sensing [21].

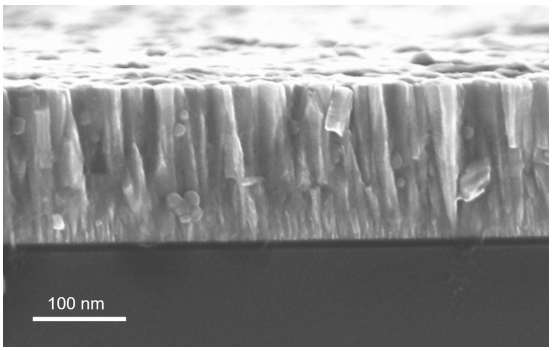

Fig. 1. SEM images of ZnO film grown on Si substrate.

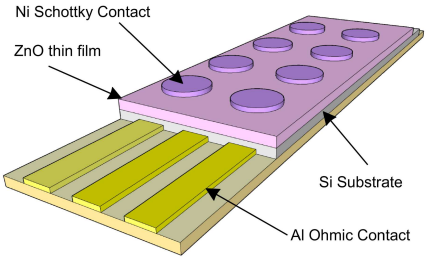

Fig. 2. Scheme of the device of Ni/ZnO Schottky diodes.

On the contrary, nickel (Ni) contacts demonstrate both rectifying and ohmic behaviour depending on the thermal annealing and surface polarity of ZnO [22]. Alivov et al. [23], reported an improvement in the rectification and ideality factor after annealing at 900°C for Au/Ni Schottky diodes of ZnO grown by RF magnetron sputtering. Ni/ZnO Schottky diodes fabricated by direct current (DC) magnetron sputtering are reported by Ievtushenko et al. [24] with improved ultraviolet (UV) photo detection. In another comparative study of Au/ZnO and Ni/Au/ZnO Schottky diodes, a high forward current and small series resistance is observed in Ni/Au Schottky contacts [25]. The reported work is based on the study of frequency- and voltage-dependent electrical characteristics of Ni/ZnO Schottky diodes and extraction of interface states density. ZnO film is grown by DC magnetron sputtering on Si substrates. Current transport mechanisms are studied from current–voltage (I–V) characteristics and electronic parameters such as barrier height (ϕ_B) and ideality factor (n) are extracted. Frequency- and voltage-dependent electrical characterizations are performed. Factors responsible for non-idealities are investigated and interface states density is extracted from I–V and capacitance–voltage (C–V) measurements. The insight and understanding of their behaviour will be helpful in the realization of more efficient devices.

2. Experiment

In this study, ZnO have been deposited on n-Si substrates (15×12 mm^2) by DC magnetron sputtering in nitrogen plasma ambient. The deposition has been carried out at room temperature in a vacuum chamber with a 4 mTorr gas pressure and a DC magnetron power of 120 W. A columnar type well textured nanostructure film having a thickness of around 165 nm has been revealed in scanning electron microscopy (SEM). The SEM image in the cross-sectional view of the grown film is shown in Fig. 1. For the Schottky contact preparation, nickel (Ni) circular dots were deposited by thermal evaporation through a shadow mask. The bonding of the substrate on conductive pads assembly has been done with silver paint. The scheme of the device is shown in Fig. 2. Current–voltage (I–V) and frequency-dependent capacitance–voltage (C–V) and conductance–voltage (G/ω–V) measurements were performed at room temperature using a Keithley SCS-4200 semiconductor characterization system by placing the sample on probe station.

3. Results and discussion

A typical nonlinear rectifying behaviour is observed in the current–voltage characteristics measured at room temperature, as shown in Fig. 3. The Schottky barrier is established at the interface of nickel and n-ZnO, because a weak rectification is generally observed in ZnO/Si junctions due to large reverse leakage currents [26, 27]. The barrier height coming from the Ni/ZnO junction can be extracted by using

$$\phi_B = -\frac{k_\mathrm{B}T}{q}\,\ln\left(\frac{I_0}{A\,A^\star\,T^2}\right). \tag{1}$$

Here, A is the area ($A = 1.13 \times 10^{-2}$ cm^2), I_0 is the reverse saturation current, k_B is the Boltzmann constant ($k_\mathrm{B} = 1.38 \times 10^{-23}$ J/K), q is the electron charge, T is temperature, and $A^\star$ is a Richardson constant having the value of 32 A/(cm^2 K^2) for n-ZnO [28]. The barrier height is estimated to be 0.68 eV. The analysis of the I–V curve gives a high ideality factor (n) of 6.3 extracted from

$$n = \frac{q\,V}{k_\mathrm{B}T}\left[\ln\left(\frac{I}{I_0}+1\right)\right]^{-1}. \tag{2}$$

High values of ideality factors, often observed in ZnO Schottky diodes, are attributed to high defect densities, tunneling and recombination processes [29–31]. Furthermore, barrier inhomogenities and interfacial layer present between metal and semiconductor are also responsible for the non-ideality [32, 33]. The charge transport behaviour of Schottky diode has been studied from the $\log(I)$–$\log(V)$ characteristics under forward bias as shown in Fig. 4. Three slopes corresponding to different conduction mechanisms were observed in the logarithmic I–V plot. At low forward voltages ($V < 0.5$ V) the linear (I–V) relationship confirmed

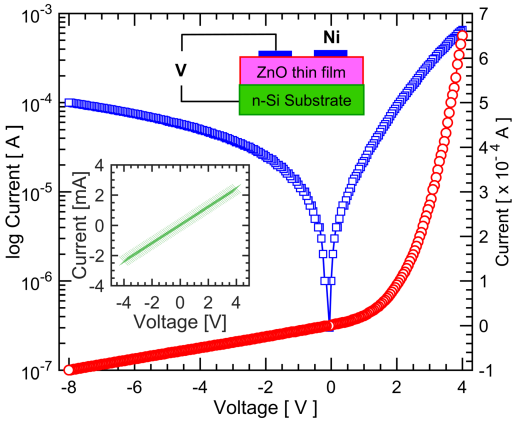

Fig. 3. The current–voltage characteristics of Ni/ZnO Schottky diode.

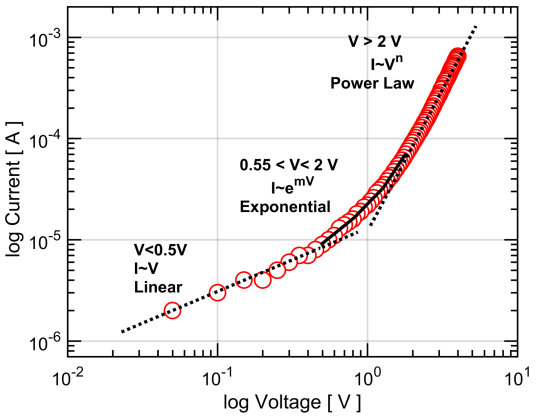

Fig. 4. The dependence of $\log(I)$–$\log(V)$ characteristics of Ni/ZnO Schottky diodes.

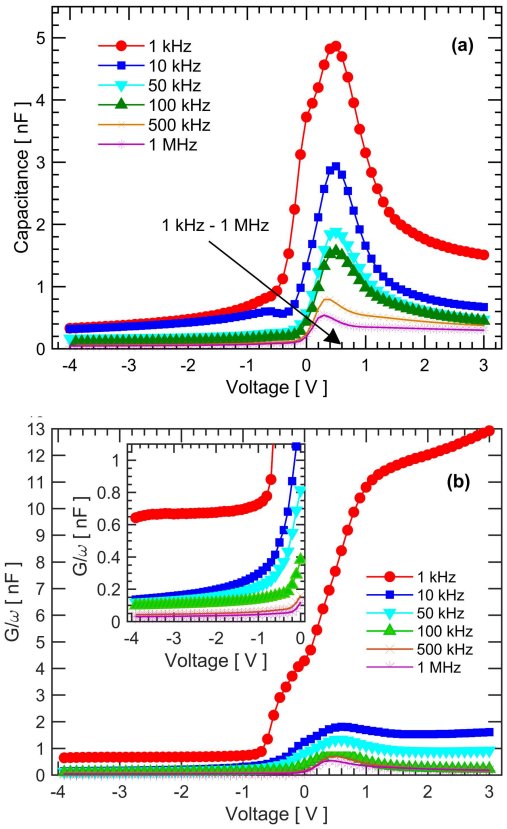

Fig. 5. Frequency and voltage dependent (a) capacitance–voltage (C–V) and (b) conductance–voltage (G/ω–V) characteristics.

the ohmic transport. The current increased exponentially ($I \sim e^{mV}$) for moderate forward voltages (0.55 V < V < 2 V), indicating that the charge transport is subjected to the space-charge-effect. For our Schottky diodes, a small value of m (1.6 V^{-1}) implies a low thermal emission of carriers induced by surface states and traps [34]. The characteristics $\log(I)$–$\log(V)$ followed power law dependence ($I \sim V^n$) at higher voltages ($V > 2$ V). Here the carrier transport approached the trap-filled limit and so the current is attributed to the trap charge limiting current (TCLC) associated with the distribution of trapped charges in the junction [35].

The frequency and voltage dependent capacitance–voltage (C–V) and conductance–voltage (G/ω–V) characterizations were carried out for a range of frequencies from 1 kHz–1 MHz at room temperature. Here ω is angular frequency given by $2\pi f$. Both the capacitance (C) and conductance (G/ω) varied with the applied voltage and frequency as shown in Fig. 5a and b. This result illustrates that C and G/ω increased with the increase in sweeping voltage (−4 V to 3 V) until they reached a peak value and then started decreasing with further increase in the applied bias. The origin of these peaks is attributed to the series resistance and interfacial defect states [18, 21]. A gradual decrease in the values of C and G/ω is observed with an increase in input AC signal frequency. This is due to the fact that interface charges easily follow the applied low-frequency AC signal and add the access capacitance, but they are unable to follow the high-frequency probe signals due the large carrier life times. Hence, their contribution is very small at higher frequencies [36, 37].

For applied reverse voltage, the relationship between the depletion layer capacitance and the applied voltage has been studied by plotting $1/C^2$ vs V for the frequency range of 1 kHz–1 MHz. Built-in potential of 0.8 is obtained from the intercept of $1/C^2$ with the voltage axis, as shown in Fig. 6. A linear dependence of $1/C^2$ vs V confirms that the carrier concentration is constant throughout the depletion region. The carrier concentration N_D equal to 2.5×10^{15} cm^{-3} is obtained from the slop of the $1/C^2$ vs V plot by using

$$N_D = \frac{2}{\varepsilon_S \varepsilon_0 \, qA^2} \frac{\mathrm{d}V}{\mathrm{d}(1/C^2)}. \qquad (3)$$

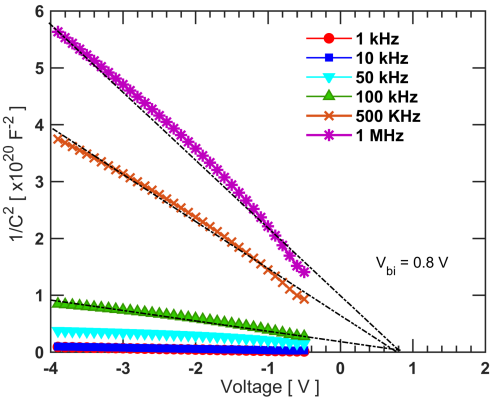

Fig. 6. The dependence of $1/C^2$ vs V for a frequency range from 1 kHz–1 MHz.

Here, A is the diode area, ε_S and ε_0 are the ZnO dielectric constant ($\varepsilon_S = 8.2$) and the vacuum constant ($\varepsilon_0 = 8.85 \times 10^{-14}$ F/cm), respectively. From the measured C–V characteristics, the barrier height is also extracted with

$$\phi_{B(C-V)} = V_{\rm bi} + \frac{k_{\rm B}T}{q} \ln\left(\frac{N_C}{N_D}\right). \quad (4)$$

Here, $V_{\rm bi}$ is a built-in potential obtained from the linear extrapolation of $1/C^2$ vs V characteristics to the voltage axis (Fig. 6). The effective density of states N_C in the conduction band (CB) is 2.94×10^{18} cm^{-3} for ZnO [38]. A barrier height of 0.98 V is obtained from (4).

The presence of interface states between metal and semiconductor plays a critical role in Schottky diodes. A non-ideal behaviour with a high ideality factor, low barrier height and rectification factor are associated with the insulating interfacial layer introduced due to oxidation of semiconductor surfaces, hydrogen, surface dipoles and incomplete covalent bonds [39, 40].

The density of interface states can be extracted from the measured I–V and C–V characteristics by using

$$N_{SS} = \frac{1}{q}\left[\frac{\varepsilon_i}{\delta}\Big(n(V) - 1\Big) - \frac{\varepsilon_S}{W_D}\right]. \quad (5)$$

Here, $n(V)$ is the voltage dependent ideality factor, W_D is the width of depletion region, and δ is the thickness of the interfacial layer. Taking into account the series resistance (R_S), the barrier height ($\phi_{\rm bo}$) and the effective barrier height (ϕ_e), the energy difference $E_C - E_{SS}$ is obtained by using

$$E_C - E_{SS} = q\big(\phi_e - V\big), \quad (6)$$

where

$$\phi_e = \phi_{\rm bo} + \left(1 - \frac{1}{n\,(V)}\right)(V - I\,R_S). \quad (7)$$

The distribution of interface states below the conduction band is shown in Fig. 7 (red line). A decrease in the interface states density given by (5) is observed in the range 1.74×10^{12}–1.87×10^{11} eV^{-1} cm^{-2} from from $E_C - 0.51$ eV to $E_C - 0.64$ eV below the conduction band.

TABLE I

Comparison of extracted N_{SS} with the previous work.

Device	N_{SS} [eV^{-1} cm^{-2}]	Ref.
Pd/ZnO	3×10^{12}	[42]
Ag/ZnO	1.72×10^{13}–1.68×10^{12}	[43]
PtO$_X$/ZnO	5.13×10^{12}	[44]
Au/ZnO/n-Si	4.25×10^{15}–1.7×10^{15}	[45]
Au/ZnO/n-Si	2.68×10^{11}	[46]
Au/(ZnO-PVA)/n-Si	6.27×10^{11}–2.23×10^{12}	[47]
Au/ZnO/p-InP	1×10^{13}–1×10^{11}	[48]
Ni/ZnO/n-Si	1.74×10^{12}–1.87×10^{11}	[this work]
	0.53×10^{12}–0.12×10^{12}	

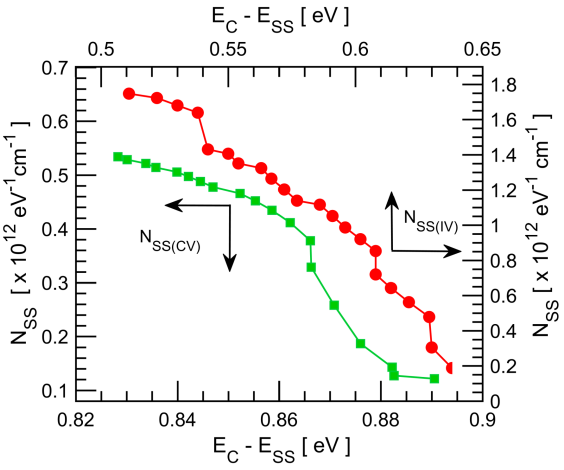

Fig. 7. Energy distribution of interface states obtained from I–V and C–V characteristics.

The interface states density N_{SS} is also extracted from high- and low-frequency capacitance characteristics by using [41]

$$N_{SS} = \sqrt{\frac{\varepsilon_S\, N_D}{2q\,\psi_S}}\left(\frac{C_{LF} - C_{HF}}{C_{HF}}\right). \quad (8)$$

Here, C_{HF} and C_{LF} are high- and low-frequency capacitances, respectively. The surface potential ψ_S is obtained from

$$\psi_S = \phi_B - \frac{k_{\rm B}T}{q}\ln\left(\frac{N_C}{N_D}\right) - \frac{V - I\,R_s}{n}. \quad (9)$$

The interface states density obtained from the capacitance–frequency (C–f) characteristics varied from 0.53×10^{12}–0.12×10^{12} eV^{-1} cm^{-2} from $E_C - 0.82$ eV to $E_C - 0.89$ eV below the conduction band edge (E_C), as shown in Fig. 7 (green line). The interface states are found high near the conduction band edge and decreased monotonically with energy approaching the center of the energy gap.

The extracted interface states densities are compared with other reported densities as shown in Table I. There are several reports on the interface state densities in ZnO contacts, therefore the estimated N_{SS} of our device may not be directly compared with the literature. However, our

estimated values are in agreement with other reported densities for ZnO metal contacts realized by various growth or deposition methods.

These surface states affect the electrical behaviour of diodes by trapping the electrons excited to the conduction band. For this reason, a complete description of interface properties is important for the realization of electronic devices with improved junction performance and reduced recombination.

4. Conclusion

The voltage- and frequency-dependent electrical characteristics and the interface state density are reported for Ni/ZnO Schottky diodes fabricated from ZnO thin films grown by DC magnetron sputtering. Electrical characterizations are performed by the I–V, C–V and G/ω–V measurements, and the barrier height, ideality factor and carrier concentration are extracted. Current transport mechanisms and possible reasons responsible for non-idealities are investigated. The densities of interface states are extracted as a function of $E_C - E_{SS}$. The results are found to be in the range 1.74×10^{12}–1.87×10^{11} eV^{-1} cm^{-2} from 0.51–0.64 eV below the conduction band edge. The interface states density obtained from capacitance–frequency (C–f) characteristics varied from 0.53×10^{12}–0.12×10^{12} eV^{-1} cm^{-2} from $E_C - 0.82$ to $E_C - 0.89$ eV below the conduction band. ZnO Schottky contacts are often far from ideal. Therefore, the investigation of the frequency- and voltage-dependent electrical characteristics, a complete description of the current transport and interface properties are very crucial for the realization of good quality Schottky diodes for design and implementation of high performance electronic circuits and systems.

Acknowledgments

The authors acknowledge the support and facilities by the Sultan Qaboos Oman IT chair office and Electronic Design Center at the NED University of Engineering and Technology for electrical characterization. The authors would like to thank Dr. Erik Khranovskyy, CEO, Grafren AB, for technical discussion and help with this work.

References

[1] V. Kumar, S.K. Singh, H. Sharma, S. Kumar, M.K. Banerjee, A. Vij, *Physica B Condensed Matter* **552**, 221 (2019).

[2] T. Mouet, T. Devers, A. Telia, Z. Messai, V. Harel, K. Konstantinov, I. Kante, M.T. Ta, *Appl. Surf. Sci.* **256**, 4114 (2010).

[3] S. Iftimie, R. Mallet, J. Merigeon, L. Ion, M. Girtan, S. Antohe, *Dig. J. Nanomater. Biostructures* **10**, 221 (2015).

[4] J.C.A.D. Queiroz, J.B.D.A. Filho, M.C. Feitor, M.S Libório, E.J.D.C. Santos, U.B. Souto, R.R.M. de Sousa, T.H.D.C. Costa, *Phys. Status Solidi (a)* **217**, 2000167 (2020).

[5] M. Chaves, R. Ramos, E. Martins, E.C. Rangel, N.C.D. Cruz, S.F. Durrant, J.R.R. Bortoleto, *Mater. Res.* **22**, (2019).

[6] M.A. Fraga, H. Furlan, R.S. Pessoa, M. Massi, *Microsys. Technol.* **20**, 9 (2014).

[7] R.C. Hoffmann, S. Sanctis, M.O. Liedke, M. Butterling, A. Wagner, C. Njel, J.J. Schneider, *Chem. Eur. J.* **27**, 5422 (2021).

[8] M. Socol, N. Preda, C. Breazu, C. Florica, A. Costas, C.M. Istrate, A. Stanculescu, M. Girtan, F. Gherendi, *Vacuum* **154**, 366 (2018).

[9] J. Chawich, W.M. Hassen, C. Elie-Caille, T. Leblois, J.J. Dubowski, *Biosensors* **11**, 145 (2021).

[10] A. Wibowo, M.A. Marsudi, M.I. Amal, M.B. Ananda, R. Stephanie, H. Ardy, H.L.J. Diguna, *RSC Adv.* **10**, 42838 (2020).

[11] M. Theuring, M. Vehse, K. von Maydell, C. Agert, *Thin Solid Films* **558**, 294 (2014).

[12] G. Georgiadou, J. Semple, A.A. Sagade, H. Forstén, P. Rantakari, Y.H. Lin, F. Alkhalil, A. Seitkhan, K. Loganathan, H. Faber, T.D. Anthopoulos, *Nat. Electron.* **3**, 718 (2020).

[13] A.B. Yadav, A. Pandey, S. Jit, *IEEE Electron. Device Lett.* **35**, 729 (2014).

[14] M.A.M. Ahmed, W.E. Meyer, J.M. Nel, *Mater. Sci. Semiconduct. Proc.* **103**, 104612 (2019).

[15] Ş. Aydoğan, K. Çınar, H.Asıl, C. Coşkun, A. Türüt, *J. Alloys Compd.* **476**, 913 (2009).

[16] A. Shokri, L. Dejam, *Int. Nano Lett.* **9**, 161 (2019).

[17] M.R. Singh, M. Sahni, M. Singh, B. Bhattacharya, N. Kumar, *J. Mater. Sci. Mater. Electron.* **30**, 13280 (2019).

[18] T. Varma, C. Periasamy, D. Boolchandani, *Superlattices Microstruct.* **112**, 151 (2017).

[19] S.M. Faraz, O. Nur, M. Willander, Q. Wahab, *IOP Conf. Ser. Mater. Sci. Eng.* **34**, 012006 (2012).

[20] T. Küçükömeroğlu, S. Yılmaz, İ. Polat, E. Bacaksız, *J. Mater. Sci. Mater. Electron.* **29**, 10054 (2018).

[21] L. Rajan, C. Periasamy, V. Sahula, *IEEE Trans. Nanotechnol.* **15**, 201 (2016).

[22] K.G. Saw, S.S. Tneh, G.L. Tan, F.K. Yam, S.S. Ng, Z. Hassan, *PLOS ONE* **9**, 86544 (2014).

[23] Y.I. Alivov, X. Bo, S. Akarca-Biyikli, Q. Fan, J. Xie, N. Biyikli, K. Zhu, D. Johnstone, H. Morkoç, *J. Electron. Mater.* **35**, 520 (2006).

[24] A. Ievtushenko, G. Lashkarev, V. Lazorenko, V. Karpyna, V. Sichkovskyi, L. Kosyachenko, V. Sklyarchuk, O. Sklyarchuk, V. Bosy, F. Korzhinski, A. Ulyashin, *Acta Phys. Pol. A*, **114**, 1123 (2008).

[25] B. Kinaci, T. Asar, S.Ş. Çetin, Y. Özen, K. Kizilkaya, *J. Optoelectron. Adv. Mater.* **14**, 959 (2012).

[26] S. Majumdar, S. Chattopadhyay, P. Banerji, *Appl. Surf. Sci.* **255**, 6141 (2009).

[27] X.Y. Ma, P.L. Chen, D.S. Li, D.R. Yang, *Solid State Phenom.* **131**, 625 (2008).

[28] S.M. Faraz, H.R. Khan, W. Shah, Q. ul Wahab, O. Nur, *Open Phys.* **19**, 467 (2021).

[29] D. Somvanshi, S. Jit, *J. Nanoelectron. Optoelectron.* **13**, 62 (2014).

[30] L. Rajan, C. Periasamy, V. Sahula, in: *2017 Conf. on Emerging Devices and Smart Sys. (ICEDSS)*, 2017, p. 63.

[31] J. Jin, J.S. Wrench, J.T. Gibbon, D. Hesp, A. Shaw, I.Z. Mitrovic, N. Sedghi, L.J. Phillips, J. Zou, V.R. Dhanak, P.R. Chalker, *IEEE Trans. Electron Devices* **64**, 1225 (2017).

[32] L. Rajan, C. Periasamy, V. Sahula, *Perspect. Sci.* **8**, 66 (2016).

[33] C.C. Cheng, J.Y. Zhan, Y.M. Liao, T.Y. Lin, Y.P. Hsieh, Y.F. Chen, *Appl. Phys. Lett.* **109**, 053501 (2016).

[34] D. Sang, Q. Wang, Q. Wang, D. Zhang, H. Hu, W. Wang, B. Zhang, Q. Fan, H. Li, *RSC Adv.* **8**, 28804 (2018).

[35] S.M. Faraz, S.R.U.N. Jafri, Z. Tajvar, N.H. Alvi, Q.U. Wahab, O.Nur, *Elektron. Elektrotech.* **27**, 49 (2021).

[36] S.M. Faraz, M. Mazhar, W. Shah, H. Noor, Z.H. Awan, M.H.Sayyad, *Physica B: Condens. Matter* **602**, 412567 (2021).

[37] D. Korucu, A. Turut, R. Turan, Ş. Altindal, *Mater. Sci. Semiconduct. Proc.* **16**, 344 (2013).

[38] M.W. Allen, M.M. Alkaisi, S.M. Durbin, *Appl. Phys. Lett.* **89**, 103520 (2006).

[39] B.G. Streetman, S.K. Banerjee, *Solid State Electronic Devices*, Prentice Hall, India 2001.

[40] L.J. Brillson, H.L. Mosbecker, M.J. Hetzer, Y. Strzhemechny, G.H. Jenssen, D.C. Look, G. Cantwell, J. Zhang, J.J. Song, *Appl. Phys. Lett.* **90**, 102116 (2007).

[41] A. Sellai, M. Mamor, S. Al-Harthi, *Surf. Rev. Lett.* **14**, 765 (2007).

[42] R.N. Gayen, S.R. Bhattacharyya, P. Jana, *Semicond. Sci. Technol.* **29**, 095022 (2014).

[43] H. Kim, H. Kim, D.W. Kim, *J. Korean Phys. Soc.* **63**, 2034 (2013).

[44] J. Jin, J. Zhang, A. Shaw, V.N. Kudina, I.Z. Mitrovic, J.S. Wrench, P.R. Chalker, C. Balocco, A. Song, S. Hall, *J. Phy. D Appl. Phys.* **51**, 065102 (2018).

[45] A. Kocyigit, I. Orak, Z. Çaldıran, A. Turut, *J. Mater. Sci. Mater. Electron.* **28**, 17177 (2017).

[46] A. Nikravan, Y. Badali, S. Altındal, I. Uslu, I. Orak, *J. Electron. Mater.* **46**, 5728 (2017).

[47] S. Nezhadesm-Kohardafchahi, S. Farjami-Shayesteh, Y. Badali, Ş. Altındal, M.A. Jamshidi-Ghozlu, Y. Azizian-Kalandaragh, *Mater. Sci. Semicond. Process.* **86**, 173 (2018).

[48] F.Z. Acar, A. Buyukbas-Ulusan, A. Tataroglu, *J. Mater. Sci.: Mater. in Electron.* **29**, 12553 (2018).